Determination of flow velocities using fiber-optic temperature measurements

Tom Renner[1], David Lah[2,*], Thomas Trick[1], Jochen Kriegseis[2]

1: Solexperts AG, 8617 Mönchaltorf, Switzerland
2: Institute of Fluids Mechanics (ISTM), Karlsruhe Institute of Technology, Germany
*Corresponding author: david.lah@kit.edu

Keywords: PIV processing, Micro PIV, Microfluidics, Heat transfer

ABSTRACT

A novel flow measuring technique is introduced to measure under harsh circumstances in environments with dirt, high pressures and elevated temperatures as in boreholes within the earth's crust. A glass fiber embedded in a cable with heating wires measures the temperature within the heated cable with distributed temperature sensing (DTS). Similar to Hot Wire Anemometry, the velocity dependence of convective heat transfer is exploited to measure the velocity of the cable as a cylinder in crossflow. A borehole-mimicking test rig and a realistic prototype of a borehole probe were built and the flow along the borehole axis was investigated. The expected Nusselt Reynolds characteristic of a cylinder in crossflow has been measured which proves the concept of this novel measurement technique.
Challenges arise with the insufficient spatial resolution of DTS measurements and in the heat transfer modeling because the temperature profile of the cables cross-section must be taken into account. More detailed investigations and developments are planned to elevate this measurement technique from the current proof-of-concept stage to a reliable flow measurement technique. As a first step, the DTS technique will be extended the application of fiber Bragg grating (FBG) temperature measurements at specific points along the glass fiber. Subsequently a straight segment of a new hybrid cable will be placed in a water channel perpendicular to the flow direction. The Flow will be precisely specified using Particle Image Velocimetry and multiple temperature sensors in the channel and on the cable's sheath will deliver the information for enhanced heat transfer modelling.

1. Background and Objectives

A wide range of large scale liquid flow-measurement situations is characterized by extremely challenging environmental conditions, which in turn limits the number of measurable quantities and accordingly diminishes the extractable information content for a given measurement campaign. These conducted experimental efforts mostly have do deal with extremely difficult optical and mechanical access, as well as particularly adverse thermal and chemical conditions, as encountered e.g. in hydrological field tests, geothermal reservoir exploration and pipeline monitoring (see e.g. Gillette & Kolpa, 2008; Klepikova et al., 2014; Bauer, 2014; Helbig & Zarrouk, 2012; Renner

& Messar, 2006). In geothermal plants, for instance, heat reservoirs located in the earth's crust are used to generate electrical energy and heating energy from the natural heat of the earth. An important method for investigating heat reservoirs is the measurement of volume flow in boreholes that penetrate a heat reservoir. Furthermore, the desired spatially distributed flow-diagnostic remains yet to be improved for an advanced analysis of the respective flow scenarios, where today the distributed quantification of volume fluxes and corresponding flow velocities appears rather premature as compared to the more elaborated means for a distributed investigation of state variables such as temperature, for instance.

Fiber-optic based distributed temperature sensing (DTS) has been developed since the 1980s, initially being used as a downhole tool for oil and gas. DTS has shown to be a precise yet robust tool for spatially distributed temperature measurements (Kersey, 2000; Li et al., 2004; Ukil et al., 2011). Research of the last two decades has led to great improvements in measurement resolution, applicability and affordability, so that DTS is now more and more frequently used to investigate hydrological systems (see Selker et al., 2006; Hausner et al., 2011; Banks et al., 2014; Bense et al., 2016). Particularly, DTS-evaluation approaches on the grounds of the temperature sensitive Raman anti-Stokes backscatter enjoy increasing attention and gain importance in the community, where the application of heated fiber cables (i.e. so-called *hybrid* cables comprised of fiber optics and high-resistance conductors) further increases the signal-to-noise-ratio as elaborated by Briggs et al. (2012); Banks et al. (2014); Bense et al. (2016) and Van De Giesen et al. (2012), for instance. Their applications range from the evaluation of groundwater flow into streams to downhole heat pulse tests, but remain largely limited to temperature-distribution quantification along the cable, thus inside the boreholes.

Note, that the general measurement strategy of DTS is comparable to Doppler-Lidar systems (Light detection and ranging), since either approach emits laser bursts and determines the distance to the observed location from the latency between burst emission the arrival of the scattered light (cp. Fernando et al., 2007). In contrast to the Doppler-based velocity determination (for the Lidar approach), the DTS approach evaluates the ratio between anti-Stokes and Stokes scatter intensities to estimate the local temperature for the given scatter location inside the fiber-optic cable. Interestingly, a heated *cable* in cross flow and the corresponding interrelationships between kinematic and thermodynamic conditions of the surrounding flow are well-known and extensively elaborated in the context of flow measurements via hot-wire anemometry (HWA) (see e.g. Stainback & Nagabushana, 1993; King, 1915; Comte-Bellot, 1976; Bruun, 1995, for more details on HWA).

The objective of the present work, therefore, revolves around the idea to treat data as received from classical fiber-optical thermography (DTS) in a similar way as the well established thermal anemometry (HWA) so as to convert the recorded Raman scatter from the fiber-optic cables into distributed velocity information inside (geothermal) boreholes and aquifers. It is accordingly hypothesized that advanced post-processing of the DTS signals received through fiber-optic cables can take immediate advantage of the known heat transfer law of cylinders in cross flow, given the sensor cable is appropriately wound around a borehole-sensor probe. To test this hypothesis, the

similarities of either measurement technique (DTS and HWA) and inherently involved limitations of the hot-wire analogy for an advanced DTS post-processing in borehole flows are outlined in a combined analytical/experimental feasibility study. For the sake of limited experimental and fabrication complexity of a borehole-mimicking test rig, the current proof-of-concept experiments exclude transverse aquifer flow across the boreholes and solely concentrate on the axial velocity around sensor probes along boreholes.

2. Experimental and Analytical Procedure

A cartoon of the applied hybrid cable and it's wound arrangement around a double-packer probe is shown in Figure 1. As indicated in Figure 1(a), the cable mimics a heated cylinder in cross flow, where the cross-flow direction of the velocity u is aligned with the borehole axis z_B. For orientation purposes both cylindrical coordinate systems for the cable ($r-\phi-z$) and the borehole ($r_\mathrm{B}-\phi_\mathrm{B}-z_\mathrm{B}$) are displayed. The cable is supplied with the electric power P_el, which is converted to heat in the high-resistance conductors of the hybrid cable. Accordingly, it may increase the cable temperature T and is converted into convective and conductive heat fluxes, the latter being mostly significant at regions with large temperature gradients along the cylinder axis, e.g. when the cable enters the water from the air. Radiation phenomena are excluded for brevity.

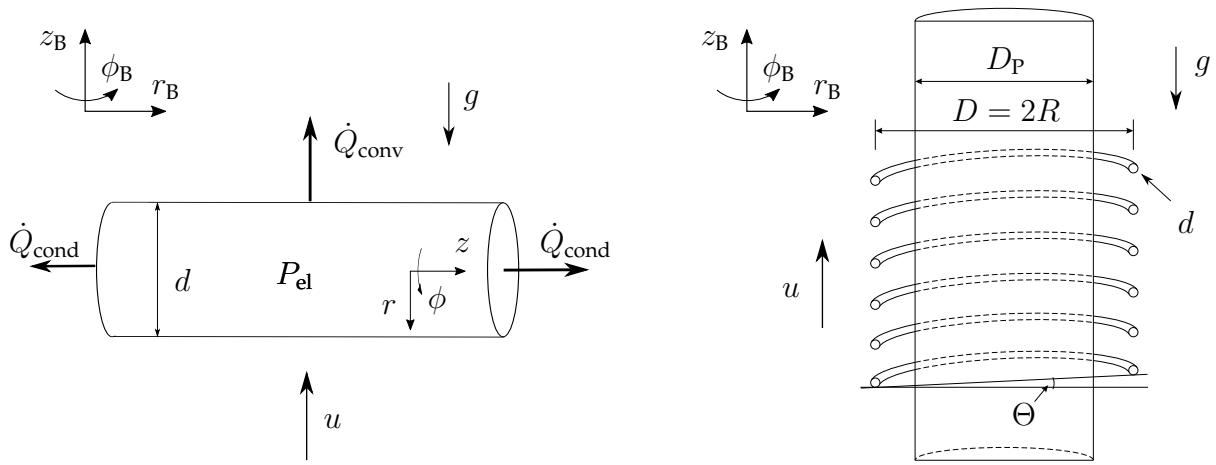

(a) hybrid cable

(b) section of the probe

Figure 1. Sketch and relevant quantities of the considered simplified double-packer probe equipped with a hybrid fiber-optic cable; (a) cable and involved thermal quantities, (b) cable orientation around a double-packer probe section.

The cable is wound helically with diameter D and angle Θ around a simplified double-packer borehole probe (cf. Solexperts-AG, 2015) with sufficient spacing $(D - D_\mathrm{P})/2$ to ensure an undisturbed flow around the probe of diameter D_P, cf. Figure 1(b). The equipped probe is inserted into the borehole-mimicking test rig as displayed in Figure 2. This test rig consists of a drainpipe with Diameter D_B and Length L_B as the borehole section, which is vertically mounted in a large water

tank. Various circumferentially oriented holes at the bottom of the pipe and the insertion of a *Linn MXH* pump result in a vertically circulating water flow rate $\dot{V}$ through the pipe against gravity g. Flow rate $\dot{V}$ and water temperature T_∞ are measured with a *Kobold Messring MIN1220* flow meter attached to the hose between the pipe and the pump.

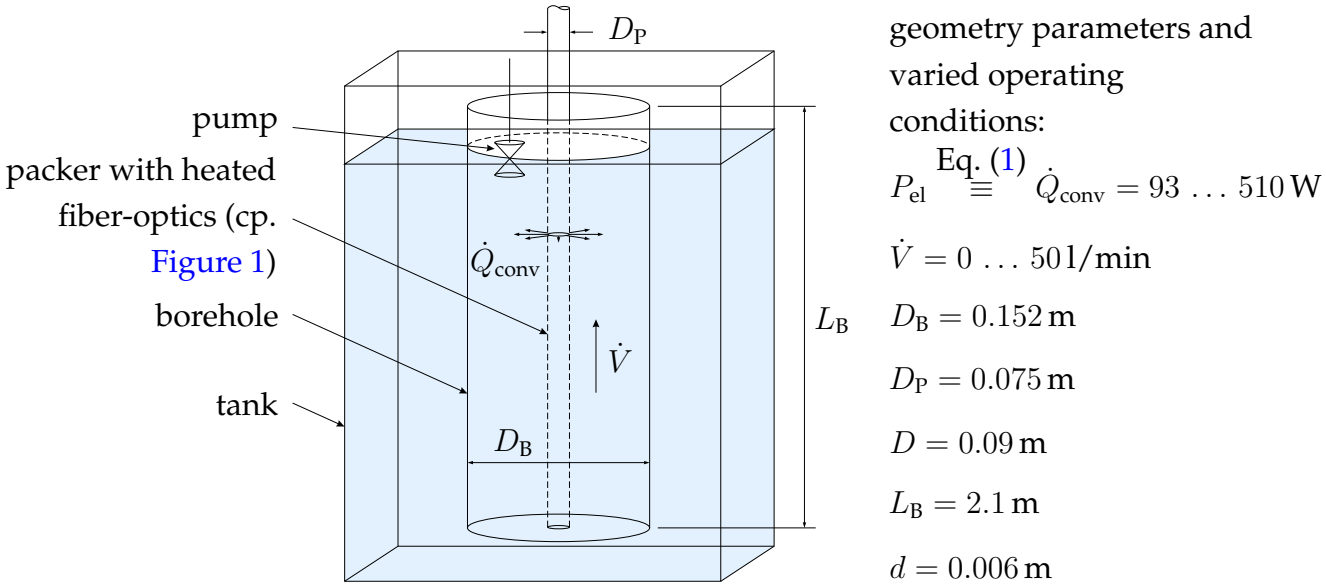

Figure 2. Sketch of the bore-hole test rig at ISTM comprised of a big water tank, a bore-hole section, a simplified double-packer probe as carrier for the hybrid DTS cable and a pump; geometry and operating parameters are added to the sketch for clarity.

The combination of energy equation, Fourier's law of heat transfer and Nusselt correlations leads to a measurement equation according to $u = f(P_\mathrm{el}, T)$ between the desired velocity information u, the given input power P_el and the cable-surface temperature T. An *AP-sensing N43856B* DTS system is used to supply the fiber optic cable with laser bursts, record the Raman scatter and convert the signals to temperature estimates, which are assumed to be constant across the cable cross-section.

If only convective heat transfer $\dot{Q}_\mathrm{conv}$ from the cable to the fluid is considered, the steady energy equation around the horizontal cylinder yields

$$0 = P_\mathrm{el} - \dot{Q}_\mathrm{conv}. \tag{1}$$

Radiative heat transfer from the cylinder to the fluid is several magnitudes smaller than the convective heat transfer and is therefore neglected. Conductive heat transport along the cylinders axis is neglected, because it is only relevant at regions with temperature gradients along the cylinder axis i.e. at the water-air boundary of the cable, which in the present setup is sufficiently far away from the investigated cable section (see Örlü & Vinuesa, 2017). Fourier's law of heat transfer relates the transferred heat $\dot{Q}_\mathrm{conv}$ to the temperature difference $\Delta T = T - T_\infty$ of the cylinders wall and the fluid, with the lateral surface $A = \pi\, d\, l$ of the cable with length l and the heat-transfer

coefficient α, i.e.

$$\dot{Q}_{\mathrm{conv}} = \alpha A (T - T_\infty) \overset{\text{Eq. (1)}}{=} P_{\mathrm{el}}. \tag{2}$$

The Reynolds number for the given problem is built with the velocity

$$u = \dot{V} \frac{4}{\pi (D_{\mathrm{B}}^2 - D_{\mathrm{P}}^2)} \tag{3}$$

and kinematic viscosity ν of the water, and the cable diameter d,

$$Re = \frac{ud}{\nu}. \tag{4}$$

The Nusselt number consists of α, d and the heat conductivity λ of the fluid,

$$Nu = \frac{\alpha d}{\lambda} \overset{\text{Eq. (2)}}{=} \frac{P_{\mathrm{el}}}{\pi l \lambda \Delta T} = \frac{C_1 P_{\mathrm{el}}}{\Delta T}, \tag{5}$$

and the Grashof number

$$Gr = \beta \Delta T \frac{g d^3}{\nu^2} = C_2 \Delta T \tag{6}$$

furthermore comprises gravity g and the thermal expansion coeffient β of the water. Note that C_1 and C_2 summarize the constant parameters in Eq. (5) and Eq. (6), respectively. Additional consideration of the ratio between kinematic viscosity ν and thermal diffusivity a via the Prandtl number

$$Pr = \frac{\nu}{a} \tag{7}$$

leads to empirical correlations in the form of $Nu = f(Re,\, Gr,\, Pr)$ for the above-mentioned measurement equation $u = f(P_{\mathrm{el}}, T)$.

Grashof and Reynolds numbers are dimensionless products describing the driving forces of the flow. Here they are used to distinct between natural and forced convection. In case of free convection, the flow is dominated by buoyancy forces and described by the Grashof number: $Nu = f(Gr,\, Pr)$. In the case of forced convection, the flow is described by the Reynolds number: $Nu = f(Re,\, Pr)$. According to Collis & Williams (1959) free convection can be neglected for $Re > Gr^{1/3}$ (see also Durst, 2008), which holds true for all parameter combinations with operating pump. Consequently, the remainder of the derivation concentrates on forced convection. The most common correlation used for hot-wire anemometry is the so-called *King's law* (cp. King, 1915)

$$Nu = \frac{1}{\pi} + \sqrt{\frac{2}{\pi}} \sqrt{RePr}, \tag{8}$$

which is valid for $Re\,Pr > 0.08$. Combination of equations Eq. (1) – Eq. (8) then results in the desired measurement equation

$$u = \frac{a}{2\pi d} \left(\frac{P_{\mathrm{el}}}{\lambda l (T - T_\infty)} - 1 \right)^2 \tag{9}$$

Equation Eq. (9) has been tested for various parameter combinations of input power and flow rates in the range of $P_{\mathrm{el}} = 93 - 510\,\mathrm{W}$ and $\dot{V} = 0 - 50\,\mathrm{l/min}$ ($Re = 0 - 365$), as will be discussed below.

3. Discussion and Conclusions

The observed interplay between normalized flow rate through the borehole and the measured temperature difference $\Delta T = T - T_\infty$ between cable and flow, thus heat transfer $\dot{Q}_{\text{conv}}$, is shown in Figure 3 with additional parametrization of the supplied electric input power. The $Re - Nu$ diagram of Figure 3(a) reveals the typical square-root shaped curves with decreasing slopes for larger Reynolds numbers. This functional relationship $Nu \sim \sqrt{Re}$ is most salient for the $P_{\text{el}} = 510\,\text{W}$−curve and confirms the general validity of the above *cylinder-in-cross-flow* assumption for further post-processing of the DTS-data in view of velocity estimates. However, it is important to mention that the determined Nusselt numbers are an order of magnitude below Kings law Eq. (8), which implies a significant overestimation of ΔT. The assumption of a homogeneous temperature distribution across the cable cross-section, therefore, must be retro-actively considered an oversimplification for the given problem.

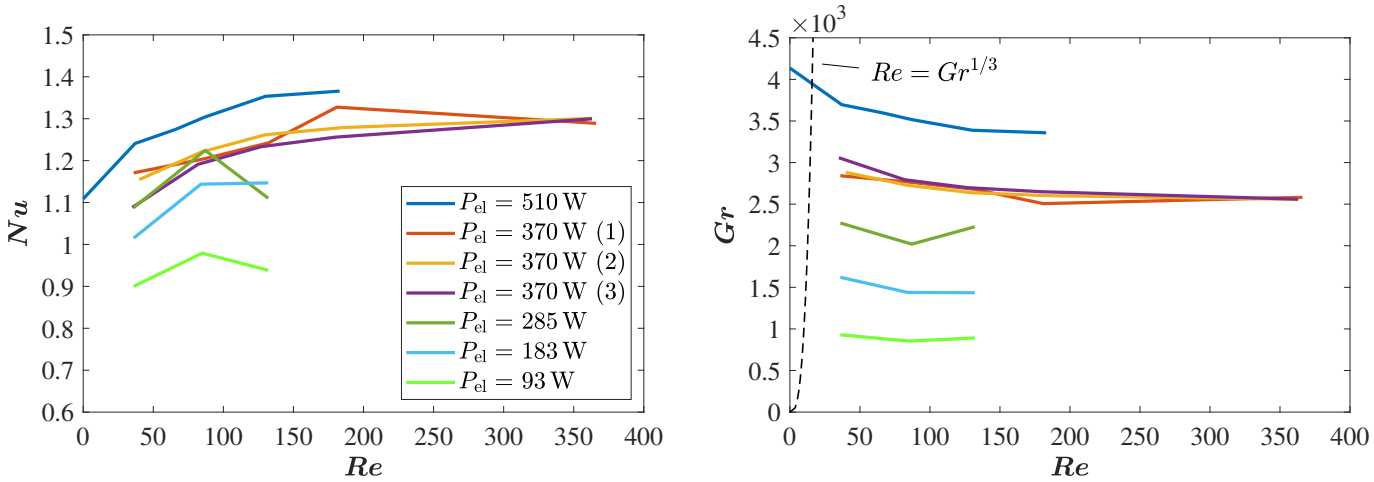

(a) Nusselt – Reynolds diagram

(b) Grashof – Reynolds diagram

Figure 3. Non-dimensional depiction of the measured temperature differences for the tested combinations of flow rate $\dot{V}$ and electric input powers P_{el}: (a) Nusselt – Reynolds diagram connects velocity with temperature difference, see measurement equation Eq. (9); (b) Grashof – Reynolds diagram indicates the influence of natural convection on the given problem.

Consequently, future efforts will also include steady heat transfer analysis with the Biot number Bi as an insightful ratio between heat-conduction resistance inside the cables and the heat-convection resistance at the cable surface. For hot-wire applications the heat-convection resistance is dominant, which is equivalent to $Bi \ll 1$ and the justification for the assumption of a constant temperature across the wires cross section. However, for the hybrid cable the Biot number increases by several orders of magnitude as demonstrated with the following estimation.

Assuming the similarity of a cylinder in cross flow with identical Nusselt and Reynolds numbers for both applications, the Biot-number change can be calculated for both cases with the values given in Table 1.

Table 1. The values for the Biot number calculation of the hybrid cable and the hot-wire are the characteristic length L, the heat conductivity of the surrounding fluid (water and air) λ_{fl}, the heat conductivity of the wall (cable isolation and wolfram) λ_{w} and wall thickness s.

	L [m]	λ_{fl} [W/(mK)]	λ_{w} [W/(mK)]	s [m]	$Bi(Nu = 1)$
hybrid cable (hc)	~10^{-3}	0.6	0.02	~10^{-3}	~30
hot-wire (hw)	~10^{-6}	0.02	70	~10^{-6}	~$3 \cdot 10^{-4}$

The Biot number is defined as

$$Bi = \frac{\alpha\, s}{\lambda_w} = \frac{Nu\, \lambda_{fl}}{L} * \frac{s}{\lambda_w} \tag{10}$$

with the heat conductivity of the wall λ_{w}, the wall thickness s and the heat transfer coefficient α, which is replaced by the Nusselt number Nu, the heat conductivity of the fluid λ_{fl} and the characteristic length scale L. The constant ratio of the hybrid cables Biot number Bi_{hc} and the hot-wires Biot number Bi_{hw} is

$$\frac{Bi_{\mathrm{hc}}}{Bi_{\mathrm{hw}}} = \underbrace{\frac{Nu_{\mathrm{hc}}}{Nu_{\mathrm{hw}}}}_{1} \underbrace{\frac{Nu_{\mathrm{hc}}}{Nu_{\mathrm{hw}}}}_{3 \cdot 10^{1}} \underbrace{\frac{\lambda_{\mathrm{w,hc}}}{\lambda_{\mathrm{w,hw}}}}_{3.5 \cdot 10^{3}} \underbrace{\frac{L_{\mathrm{hw}}}{L_{\mathrm{hc}}}}_{10^{-3}} \underbrace{\frac{s_{\mathrm{hc}}}{s_{\mathrm{hw}}}}_{10^{3}} \approx 10^{5}. \tag{11}$$

The Biot number increases by five orders of magnitude from hot-wire to hybrid cable, because of the change of fluid and the change of wall material. The increased thermal conductivity of water compared to air decreases the convective heat transfer resistance and the decreased thermal conductivity of the wall increases the heat conduction resistance. The change of the geometric length scale does not influence the Biot number, it is expected to increase the response time of the sensor in unsteady modelling.

This estimation suggests $Bi > 1$ for the hybrid cable, which indicates, that the heat-conduction resistance is dominant. Thus, most of the measured temperature difference drops within the cables sheath and the relevant temperature difference for the calculation of the Nusselt number is accordingly smaller. This effect will in turn lead to increased Nusselt-number estimates due to $Nu \sim 1/\Delta T$. Future measurements are foreseen, which therefore also include heat conduction phenomena within the cable and compare the experiments with adjusted Nusselt numbers to Kings Law. Additionally, further development of the hybrid cable will consider thinner isolation layers or materials with higher thermal conductivity to reduce the Biot number. After thoroughly discussing that a temperature difference within the cable is prevalent, it must be emphasized that it is constant in steady heat transfer. Therefore, it must be only considered for academic purposes when comparing the results to those in the literature. For practical use, however, an appropriate calibration will effectively eliminate this offset. Unsteady heat transfer is not expected in borehole applications and will accordingly not be discussed here.

The effect of buoyancy induced flows of natural convection on the measurements is shown in Figure 3(b), where now the Grashof number is plotted on the ordinate against the Reynolds number. The diagram demonstrates, that all experiments exceed the aforementioned $Re > Gr^{1/3}$ condition (see Collis & Williams, 1959), thus rendering natural convection mostly of minor importance. The only exception is the quiescent-water test run ($Re = 0$), which is buoyancy dominated as expected. Since future efforts will also consider very small Reynolds numbers (e.g. aquifer monitoring), the consideration of natural convection will not be neglected from the processing approach.

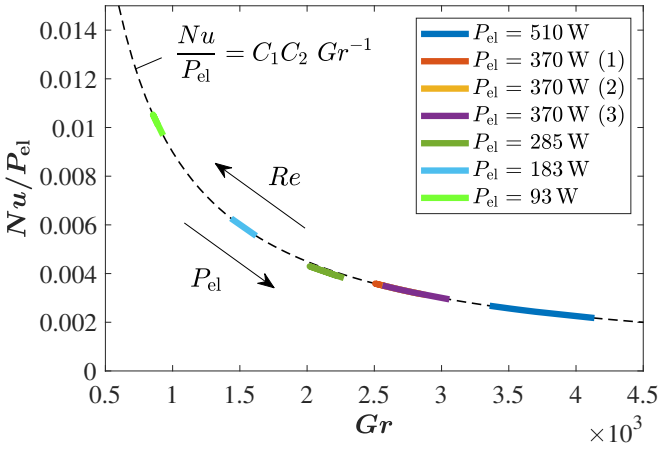

Figure 4. All measured data plotted in a $Nu/P_{el} - Gr-$diagram collapse on a single curve $C_1 C_2 Gr^{-1}$, leading to a $P_{el} - Re-$parameter map for the problem.

Even though less meaningful at first glance, the direct combination of the Grashof number Eq. (6) with the Nusselt number Eq. (5) leads to a determining equation for the constants C_1 and C_2 according to

$$\frac{Nu}{P_{el}} = \frac{1}{\pi l \lambda}\, \beta \frac{g d^3}{\nu^2}\, Gr^{-1} = C_1 C_2 Gr^{-1}. \tag{12}$$

Equation Eq. (12) is plotted in a $Nu/P_{el} - Gr-$diagram in Figure 4 (dashed line) alongside all experimental results. Note that the measured temperature difference ΔT is eliminated from the equation. Nonetheless, this diagram serves as a valuable $P_{el} - Re-$parameter map, where all measured data points theoretically collapse on a single curve. Consequently, only a single calibration experiment is required for an accurate determination of all constant parameters for a given setup.

This is an important insight for the long-term objective to apply the proposed method in harsh field conditions as outlined in Section 1, since such a calibration can be conducted prior to the borehole application under defined and adjustable boundary condition. Subsequently, the validity of all downhole measurements can be evaluated by means of an application-specific tolerated uncertainty margin around the calibrated theoretical curve in the map. From today's perspective, the product $P_{el}\, C_1\, C_2$ is interpreted as meaningful dimensionless power characteristic and will, therefore, also be subject of future investigations.

To elevate the measurement technique from the proof-of-concept level to a validated level with well-known measurement range and error margins, fundamental investigations of a straight cable

section as perfect *undisturbed-cylinder-in-crossflow* are currently prepared at ISTM in a PIV equipped water channel. Subsequently, the technique will be transferred from the lab setup to a realistic borehole probe by Solexperts. Therefore, the validity of the *undisturbed-cylinder-in-crossflow* assumption for the helical cable arrangement around the probe is to be verified with additional PIV experiments alongside the revised borehole-mimicking test rig. Comprehensive cylinder-wake and cylinder-cylinder interference flow-field investigations are expected to shed more light into the Reynolds-number dependent degree of simplification and corresponding error margins due to this assumption.

As a final technical note, the DTS system used in this work (*AP-sensing N43856B*) has a minimum spatial resolution of $0.5\,\mathrm{m}$, which renders the identification of local temperature phenomena particularly challenging. Even though obviously sufficient for the setup in the present work, due to quasi-steady temperatures along the spiral probe in vertical flow, the distinction of different temperatures around the probe perimeter in case of transverse flow across the borehole seems very difficult and expensive with standard DTS as elaborated by e.g. Thomcraft et al. (1992); Dyer et al. (2012) and Bazzo et al. (2016). The additional application of fiber Bragg gratings (FBG) is considered a promising alternative extension to the present DTS setup, which is currently implemented to the test rig at ISTM. An FBG is a very short optical grating on the fiber that responds sensitive to a very tightly constrained frequency band of light and enables point measurements of temperature (see e.g. Selker et al., 2006). The required number of included FBGs along the fiber-optic cable, i.e. around the probe perimeter, to achieve sufficient spatial resolution for transverse flows will accordingly be addressed in future investigations.

Acknowledgements

Financial support through the Central Innovation Programme for SMEs (ZIM) of the Federal Ministry of Economics and Technology (BMWi), funding grant No. KK5212601DF0 / KK5152802DF0, is kindly acknowledged.

References

Banks, E. W., Shanafield, M. A., & Cook, P. G. (2014). Induced temperature gradients to examine groundwater flowpaths in open boreholes. *Groundwater*, *52*(6), 943–951. https://doi.org/10.1111/gwat.12157

Bauer, M. (2014). *Handbuch tiefe geothermie* (W. H. Freeden, H. H. Jacobi, & T. Neu, Eds.). Berlin, Heidelberg: Springer Spektrum. https://doi.org/10.1007/978-3-642-54511-5

Bazzo, J. P., Pipa, D. R., Martelli, C., da Silva, E. V., & da Silva, J. C. C. (2016). Improving spatial resolution of raman dts using total variation deconvolution. *IEEE Sensors Journal*, *16*(11), 4425–4430. https://doi.org/10.1109/JSEN.2016.2539279

Bense, V., Read, T., Bour, O., Le Borgne, T., Coleman, T., Krause, S., ... Selker, J. (2016). Distributed temperature sensing as a downhole tool in hydrogeology. *Water Resources Research*, *52*(12), 9259–9273. https://doi.org/10.1002/2016WR018869

Briggs, M. A., Lautz, L. K., & McKenzie, J. M. (2012). A comparison of fibre-optic distributed temperature sensing to traditional methods of evaluating groundwater inflow to streams. *Hydrological Processes*, *26*(9), 1277–1290. https://doi.org/10.1002/hyp.8200

Bruun, H. H. (1995). *Hot-wire anemometry: principles and signal analysis*. Oxford University Press.

Collis, D. C., & Williams, M. J. (1959). Two-dimensional convection from heated wires at low reynolds numbers. *Journal of Fluid Mechanics*, *6*(3), 357–384. https://doi.org/10.1017/S0022112059000696

Comte-Bellot, G. (1976). Hot-wire anemometry. *Annual review of fluid mechanics*, *8*(1), 209–231. https://doi.org/10.1146/annurev.fl.08.010176.001233

Durst, F. (2008). *Fluid mechanics: an introduction to the theory of fluid flows*. Springer Science & Business Media.

Dyer, S. D., Tanner, M. G., Baek, B., Hadfield, R. H., & Nam, S. W. (2012). Analysis of a distributed fiber-optic temperature sensor using single-photon detectors. *Optics express*, *20*(4), 3456–3466. https://doi.org/10.1364/OE.20.003456

Fernando, H. J., Princevac, M., & Calhoun, R. J. (2007). Atmospheric measurements. In C. Tropea, A. L. Yarin, & J. F. Foss (Eds.), *Springer handbook of experimental fluid mechanics* (p. 1157-1178). Springer, Heidelberg. https://doi.org/10.1007/978-3-540-30299-5

Gillette, J. L., & Kolpa, R. L. (2008, 2). Overview of interstate hydrogen pipeline systems. *U.S. Department of Energy Office of Scientific and Technical Information*. https://doi.org/10.2172/924391

Hausner, M. B., Suárez, F., Glander, K. E., Giesen, N. v. d., Selker, J. S., & Tyler, S. W. (2011). Calibrating single-ended fiber-optic raman spectra distributed temperature sensing data. *Sensors*, *11*(11), 10859–10879. https://doi.org/10.3390/s111110859

Helbig, S., & Zarrouk, S. J. (2012). Measuring two-phase flow in geothermal pipelines using sharp edge orifice plates. *Geothermics*, *44*, 52–64. https://doi.org/10.1016/j.geothermics.2012.07.003

Kersey, A. D. (2000). Optical fiber sensors for permanent downwell monitoring applications in the oil and gas industry. *IEICE transactions on electronics*, *83*(3), 400–404.

King, L. V. (1915). LVII. On the precision measurement of air velocity by means of the linear hot-wire anemometer. *The London, Edinburgh, and Dublin Philosophical Magazine and Journal of Science*, *29*(172), 556–577. https://doi.org/10.1080/14786440408635334

Klepikova, M. V., Le Borgne, T., Bour, O., Gallagher, K., Hochreutener, R., & Lavenant, N. (2014). Passive temperature tomography experiments to characterize transmissivity and connectivity of preferential flow paths in fractured media. *Journal of Hydrology*, *512*, 549-562. https://doi.org/10.1016/j.jhydrol.2014.03.018

Li, H.-N., Li, D.-S., & Song, G.-B. (2004). Recent applications of fiber optic sensors to health monitoring in civil engineering. *Engineering Structures*, *26*(11), 1647-1657. https://doi.org/10.1016/j.engstruct.2004.05.018

Renner, J., & Messar, M. (2006). Periodic pumping tests. *Geophysical Journal International*, *167*(1), 479–493.

Selker, J. S., Thevenaz, L., Huwald, H., Mallet, A., Luxemburg, W., Van De Giesen, N., ... Parlange, M. B. (2006). Distributed fiber-optic temperature sensing for hydrologic systems. *Water Resources Research*, *42*(12). https://doi.org/10.1029/2006WR005326

Solexperts-AG. (2015). *information about double-packer systems.* (see www.solexperts.com)

Stainback, P., & Nagabushana, K. (1993). Review of hot-wire anemometry techniques and the range of their applicability for various flows. *Electronic Journal of Fluids Engineering*, *1*.

Thomcraft, D., Sceats, M., & Poole, S. (1992). An ultra high resolution temperature sensor'. In *Proceedings of the 8th optical fibres sensors conference, monterey, ca* (pp. 258–260). https://doi.org/10.1364/OFS.1992.Th14

Ukil, A., Braendle, H., & Krippner, P. (2011). Distributed temperature sensing: review of technology and applications. *IEEE Sensors Journal*, *12*(5), 885–892. https://doi.org/10.1109/JSEN.2011.2162060

Van De Giesen, N., Steele-Dunne, S. C., Jansen, J., Hoes, O., Hausner, M. B., Tyler, S., & Selker, J. (2012). Double-ended calibration of fiber-optic raman spectra distributed temperature sensing data. *Sensors*, *12*(5), 5471–5485. https://doi.org/10.3390/s120505471

Örlü, R., & Vinuesa, R. (2017). Thermal anemometry. In S. Discetti & A. Ianiro (Eds.), *Experimental aerodynamics* (p. 257-304). Taylor & Francis, London. https://doi.org/10.1201/9781315371733